



Numerical Computations of Transonic Critical Aerodynamic Behavior of a Realistic Artillery Projectile

Ahmed F. M. Kridi

Department of Manufacturing Operation Eng. /Al-Khwarizmi College of Eng. /University of Baghdad

(Received 31 January 2008; accepted 25 March 2009)

Abstract

The determination of aerodynamic coefficients by shell designers is a critical step in the development of any projectile design. Of particular interest is the determination of the aerodynamic coefficients at transonic speeds. It is in this speed regime that the critical aerodynamic behavior occurs and a rapid change in the aerodynamic coefficients is observed. Two-dimensional, transonic, flow field computations over projectiles have been made using Euler equations which were used for solution with no special treatment required. In this work a solution algorithm is based on finite difference MacCormack's technique for solving mixed subsonic-supersonic flow problem. Details of the asymmetrically located shock waves on the projectiles have been determined. Computed surface pressures have been compared with experimental data and are found to be in good agreement. The pitching moment coefficient, determined from the computed flow fields, shows the critical aerodynamic behavior observed in free flights.

Keywords: CFD, Euler Equation, Artillery Projectile, MacCormack's technique.

1. Introduction

The flight of projectiles covers a wide range of speeds. The accurate prediction of projectile aerodynamics at these speeds is of significant importance in the early design stage of a projectile. The critical aerodynamic behavior occurs in the transonic speed regime, $0.9 < M < 1.2$ where the aerodynamic coefficients have been found to change by as much as 100%. Of particular interest is the determination of the pitching-moment coefficient since it is used to determine the static stability of the projectile. The critical behavior in this case is usually characterized by a rapid increase in the coefficient followed by a sharp drop. This rapid change in the pitching moment coefficient can be attributed in part to the complex flow structure and, in particular, to the asymmetrically located shock waves, which exist on projectiles flying at transonic speeds at angle of attack. Computations of two-dimensional flow fields at transonic speeds are thus needed to predict the critical aerodynamic behavior. A considerable research effort has been focused on the development of modern predictive

capabilities for determining projectile aerodynamic¹⁻⁵. Numerical capabilities have been developed primarily using Euler equation computational techniques and have been used to compute flow over slender bodies of revolution at transonic speeds. Flow field computations have included both axisymmetric⁴ and two-dimensional situations.^{1, 2, 3, 5} initial computations¹⁻³ did not include the wake or base region of a projectile and, thus, ignored the upstream effect of the base region flow on the afterbody.

Benek et. al.⁶ show the development of a chimera grid scheme. This scheme provides multiple regions where communications between grids are done by interpolating in regions of overlap. A blocked grid approach reported by Belk and Whitfield⁷ does not require interpolations at the interfaces and has been successfully used to obtain Euler solutions over a wing. The scheme used by Benek et. al.⁶ is generally complicated since it allows for embedding a block or zone into another. Recently, a simple composite grid scheme has been

developed here a large single grid was partitioned into smaller grids. Each of the smaller problems was solved separately with simple data transfers at the interfaces. The initial results obtained were very promising. The present effort extends the use of this simple algebraic grid scheme to include the correct modeling of a projectile.

The aim of the present work is to study numerically the two-dimensional projectile flow field for air missiles under the conditions of free stream Mach number 0.9, 0.92, 0.94, 0.96, 0.98, 1.0, 1.1, 1.2 in transonic speed case at atmospheric conditions, pressure 101325 N/m² and temperature 15°C.

2. Theoretical Analysis

The calculation of the projectile flow field is of considerable importance to the efficient design of projectile. These flow fields are very complex due to their mixed hyperbolic-elliptic nature, the influence the forbody and viscous effects, as well as the three-dimensionality. The complexities of three-dimensional viscous inlet flow make their numerical prediction a very difficult task; therefore, the calculation of two dimensional inlets is an step toward that direction.

The projectile flow fields calculated by a two-dimensional computational method, the problem of employing an explicit, time-marching, finite difference procedure to solve the Euler equation formulated in body-fitted coordinates. The method can be used for a flow field in both supersonic and subsonic regions.

2.1. Model and Computational Grids

The model used for the computational study presented here is an idealization of a realistic artillery projectile geometry. The experimental model shown in Fig. 1 is a secant-ogive cylinder-boattail (SOCBT) projectile. It consists of a three caliber (one-caliber=maximum body diameter), sharp, secant-ogive nose, a two-caliber, cylindrical midsection, and One-caliber boattail.

The computational grid used for this computation is shown in Fig. 2 shows the longitudinal cross section of the two-dimensional grid. The algebraic equation is used to relate the grid points in the computational domain to those of the physical domain. This objective is met by using an interpolation scheme between the specified boundary grid points to generate the

interior grid points. Clearly, many algebraic equations can be introduced for this purpose.

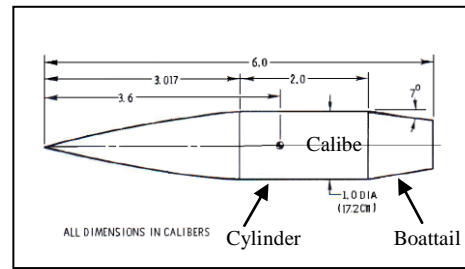


Fig.1. Model Geometry of SOCBT Projectile.

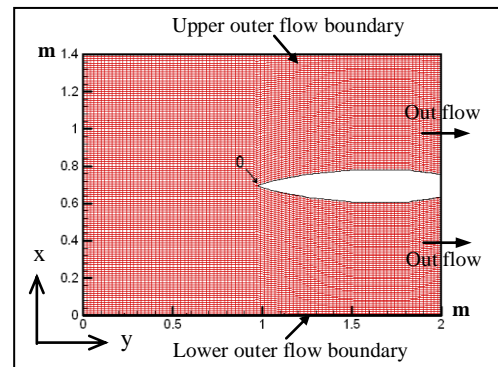


Fig.2. Two Dimension Projectile (General Shape).

2.2. Governing equations

For high Reynolds number flows, viscous effects are confined to the vicinity of the surface, where large velocity gradients exist. This region is known as the boundary layer. Outside the boundary layer, the velocity gradients are negligible resulting in zero shear stresses. This region is called the inviscid region, and solution procedures for the inviscid flow region are governed by the Euler equations and the solution of this research depends on it, which is written in conservation-law form for two-dimensional flows of a perfect gas⁸.

The general compact vector form is given as:-

$$\frac{\partial U}{\partial t} + \frac{\partial E}{\partial x} + \frac{\partial F}{\partial y} = 0,$$

Where:

$$U = \begin{bmatrix} \rho \\ \rho u \\ \rho v \\ \rho e_t \end{bmatrix}, E = \begin{bmatrix} \rho u \\ \rho u^2 + p \\ \rho uv \\ u(e_t + p) \end{bmatrix}, F = \begin{bmatrix} \rho v \\ \rho uv \\ \rho v^2 + p \\ v(e_t + p) \end{bmatrix} \dots(1)$$

u and v are the velocities along the x and y coordinates, respectively, p is the pressure, ρ is the density, and e_t is the total energy per unit volume. And U, E, F , are the fluxes vectors.

To transform the Euler Equation (1) into curvilinear coordinates (ξ, η) , an independent variable may be written as follows:-

$$\frac{\partial \bar{U}}{\partial t} = -\frac{\partial \bar{E}}{\partial \xi} - \frac{\partial \bar{F}}{\partial \eta} \quad \dots(2)$$

Where:

$$\left. \begin{aligned} \bar{U} = \frac{U}{J} &\Rightarrow U_1 = \frac{\rho}{J} \\ U_2 = \frac{\rho u}{J} &= U_1 u \\ U_3 = \frac{\rho v}{J} &= U_1 v \\ U_4 = \frac{\rho}{J} \left(e + \frac{u^2}{2} + \frac{v^2}{2} \right) &= \left(e + \frac{u^2}{2} + \frac{v^2}{2} \right) U_1 \end{aligned} \right\} \dots(2a)$$

$$\left. \begin{aligned} \bar{E} &= \frac{1}{J} (\xi_x E + \xi_y F) \Rightarrow \\ E_1 &= \xi_x U_2 + \xi_y U_3 \\ E_2 &= \xi_x (U_2 \cdot u + \frac{P}{J}) + \xi_y (U_3 \cdot u) \\ E_3 &= \xi_x (U_2 \cdot v) + \xi_y (U_3 \cdot v + \frac{P}{J}) \\ E_4 &= \xi_x (U_4 + \frac{P}{J}) \cdot u + \xi_y (U_4 + \frac{P}{J}) \cdot v \end{aligned} \right\} \dots(2b)$$

$$\left. \begin{aligned} \bar{F} &= \frac{1}{J} (\eta_x E + \eta_y F) \Rightarrow \\ F_1 &= \eta_x U_2 + \eta_y U_3 \\ F_2 &= \eta_x (U_2 \cdot u + \frac{P}{J}) + \eta_y (U_3 \cdot u) \\ F_3 &= \eta_x (U_2 \cdot v) + \eta_y (U_3 \cdot v + \frac{P}{J}) \\ F_4 &= \eta_x (U_4 + \frac{P}{J}) \cdot u + \eta_y (U_4 + \frac{P}{J}) \cdot v \end{aligned} \right\} \dots(2c)$$

where:

ρ, u, v, p and e are a (primitive variables) non dimensional density, velocity in x -direction, velocity in y -direction, pressure and internal energy respectively.

2.3. MacCormack's Technique:

The MacCormack's time marching method is an explicit finite-difference technique. It is second-order-accurate in both space and time. This method will be used to solve the Euler Equation itemized in Equations (2a) to (2c) with march in time to steady state solution by solving the flow properties at every (i, j) spatial location, assuming that the flow field at each node is known at time t .

Consider the U flow field variable at grid point (i, j) at time $t + \Delta t$. In MacCormack's method, this is obtained from

$$U_{i,j}^{t+\Delta t} = U_{i,j}^t + \left(\frac{\partial U}{\partial t} \right)_{av} \Delta t \quad \dots(3)$$

Where $(\partial U / \partial t)_{av}$ is a represented mean value of $(\partial U / \partial t)$ between time t and $t + \Delta t$. The value of $(\partial U / \partial t)_{av}$ is calculated as a second order accuracy, and once again, U is a flow field variable known at time t . Either from initial condition or as a result from the previous iteration in time. $(\partial U / \partial t)_{av}$ is defined as:

$$\left(\frac{\partial U}{\partial t} \right)_{av} = \frac{1}{2} \left[\left(\frac{\partial U}{\partial t} \right)_{i,j}^t + \left(\frac{\partial U}{\partial t} \right)_{i,j}^{t+\Delta t} \right] \quad \dots(4)$$

To obtain a value of $(\partial U / \partial t)_{av}$, produce initial fluxes from primitive variables by using Equations (2a) to (2c) and then there are two major steps taken as:-

1. Predictor step: $(\partial U / \partial t)_{i,j}^t$ is calculated using forward spatial difference on the right side of the governing equation (2) from the known flow field at time t . The predicted value of the flow field variable can be obtained at $t + \Delta t$, as follows:-

$$U_{p,i,j}^{t+\Delta t} = U_{i,j}^t - \frac{\Delta t}{\Delta \xi} (E_{i+1,j}^t - E_{i,j}^t) - \frac{\Delta t}{\Delta \eta} (F_{i,j+1}^t - F_{i,j}^t) \quad \dots(5)$$

For the interior nodes a new value of parameters (ρ, u, v, p and e) will be found from the new fluxes using equation (2a). After that, the updating boundaries must be done. From the new value of parameters that have been derived, the influence of the boundary updating flux must be done using equations (2a) through (2c).

2. Corrector step: Using backward spatial differences, the predicted value (from step 1) is inserted into the governing equation such that a

predicted time derivative $(\partial U_p / \partial t)_{i,j}^{t+\Delta t}$ can be obtained. The equation of backward space is illustrated as:-

$$U_{C_{i,j}}^{t+\Delta t} = U_{P_{i,j}}^{t+\Delta t} - \frac{\Delta t}{\Delta \xi} (E_{P_{i,j}}^{t+\Delta t} - E_{P_{i-1,j}}^{t+\Delta t}) - \frac{\Delta t}{\Delta \eta} (F_{P_{i,j}}^{t+\Delta t} - F_{P_{i,j-1}}^{t+\Delta t}) \dots(6)$$

Then, substitute $(\partial U_c / \partial t)_{i,j}^{t+\Delta t}$ and $(\partial U / \partial t)_{i,j}^t$ by equation (4) to obtain the average value, to find the corrected second order accurate value of U at time $t+\Delta t$, combining equations (4) and (6) and substituting them by equation (3) yields:-

$$U_{i,j}^{t+\Delta t} = \frac{1}{2} \left[U_{i,j}^t + U_{P_{i,j}}^{t+\Delta t} - \frac{\Delta t}{\Delta \xi} (E_{P_{i,j}}^{t+\Delta t} - E_{P_{i-1,j}}^{t+\Delta t}) - \frac{\Delta t}{\Delta \eta} (F_{P_{i,j}}^{t+\Delta t} - F_{P_{i,j-1}}^{t+\Delta t}) \right] \dots(7)$$

And from the new corrected fluxes it is possible to obtain the correct value of parameters (ρ , u , v , p and e) for all interior nodes by using equation (2a) then updating boundaries. The above steps are repeated until the flow field variable approaches a steady state value; this is the desired steady state solution.

2.4. Time Step Calculation:

The value of Δt cannot be arbitrary, rather it must be less than some maximum values for stability, it was stated that Δt must obey the Courant-Friedriches-Lowry criterion *CFL*. The *CFL* criterion states that physically the explicit time step must be not greater than the time required for a sound wave to propagate from one grid to next. The maximum allowable value of *CFL* factor for stability in explicitly time dependent finite difference calculation can vary from approximately 0.5 to 0.1. To determine the value of time step, the following version of the *CFL* criterion⁹ is used. Where $a_{i,j}$ is the local speed of sound in meters per second, and C is a constant.

$$(\Delta t_{CFL})_{i,j} = \left[\left| \frac{u_{i,j}}{\Delta \xi} \right| + \left| \frac{v_{i,j}}{\Delta \eta} \right| + a_{i,j} \sqrt{\frac{1}{\Delta \xi^2} + \frac{1}{\Delta \eta^2}} \right]^{-1} \dots(8)$$

And, $\Delta t = \min [C (\Delta t_{CFL})_{i,j}]$.

2.5. Boundary Condition:

The Euler equation has an unlimited number of solutions. What makes a solution unique is the

proper specification of initial and boundary conditions for a given *PDE* (Euler equation). A set of boundary conditions must be specified, it referred to as the “analytical boundary condition” Once the *PDE* is approximated by a *FDE*, Thus the *FDE* will require additional boundary conditions. This boundary condition will be referred to as “numerical boundary condition”. As for the problem under consideration, there are four types of boundaries: solid, inflow, outer and outflow.

2.5.1. Solid boundary Condition

For the two solid boundary conditions (projectile upper surface and lower surface), the tangency grid body surface must be satisfied for inviscid flow. The components of the momentum equation for the two-dimension flow may be expressed with some mathematical steps, as¹⁰:-

$$\left. \begin{aligned} &\eta_x \left(\frac{\rho u \bar{U}}{J} \right)_\xi + \eta_y \left(\frac{\rho u \bar{U}}{J} \right)_\xi + \eta_x \left(\frac{\rho v \bar{V}}{J} \right)_\eta + \eta_x \left(\frac{\rho u \bar{V}}{J} \right)_\eta \\ &+ \eta_x \left(\frac{\xi_x P}{J} \right)_\xi + \eta_x \left(\frac{\eta_x P}{J} \right)_\eta + \eta_y \left(\frac{\xi_y P}{J} \right)_\xi + \eta_y \left(\frac{\eta_y P}{J} \right)_\eta = 0 \end{aligned} \right\} \dots(9)$$

a. Upper projectile surface:-

A finite difference equation for the upper equation is obtained, as a second order central difference approximation for the ξ derivatives and a second order forward difference approximation for η derivatives are used.

b. Lower projectile surface:-

A second order central difference approximation for ξ derivatives and second-order backward difference approximation for η derivatives are used.

2.5.2. Outer Flow Boundary

The upper outer flow boundary is the air flow out from the numerical simulation of two-dimensional projectile at 1.4 meter in the x -direction. To calculate the properties at this boundary, first order backward transformation derivatives are used. The lower outer flow boundary is the air flow out from the numerical simulation of two-dimensional projectile at zero meter in the x -direction, the first order forward transformation derivatives are used to calculate the properties as shown in Fig. 2.

2.5.3. Out flow Boundary

The outflow boundary illustrated in Fig. 2 represents the airflow above and below the projectile. This airflow is got out from the numerical simulation and is two meters far from the original point. The air flow properties are calculated by using backward transformation derivatives.

3. Results and Discussions

The projectile characteristics at transonic speed are dominated by the shock-wave systems that go into their design. In the following results we put aside temporarily the problems of boundary layer and flow separation and consider the simple nature and properties of shock wave. The implicit time marching procedure was used to obtain the desired steady-state result. Initial conditions were free-stream everywhere, and the boundary conditions were up-dated explicitly at each time step. For (SOCBT) Projectile, $0.9 < M_{\infty} < 1.2$, Results have been obtained at various transonic speeds. Figures 3, 4, 5, 7, 8, 9 and 10 show the Mach contours for the projectile in the wind-ward and lee-ward planes. These figures show the expansions at the ogive-cylinder and cylinder-boattail. These figures indicate the presence of shock waves on the cylinder and also on the boattail, which typically occur on the projectile at transonic speeds. Sharp shocks are observed on the boattail. These boattail shocks are shown to be longitudinally asymmetric due to the influence angle of attack (4°). As the Mach number increases from 0.90 to 0.96 and then to 0.98 the shocks become stronger and move towards the base of the projectile. At higher transonic speeds past the speed of sound (see Fig. 10), these shocks become weak; however, a bow shock forms in front of the nose of the projectile.

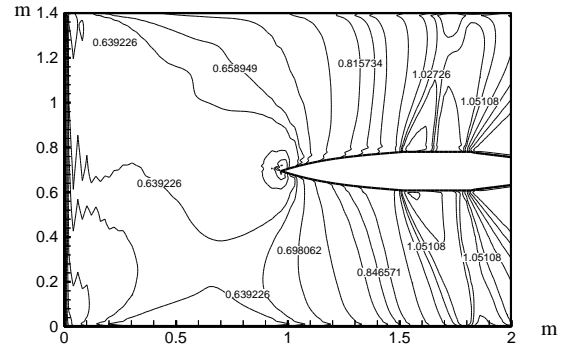


Fig. 4. Machconture, SOCBT, M=0. 92

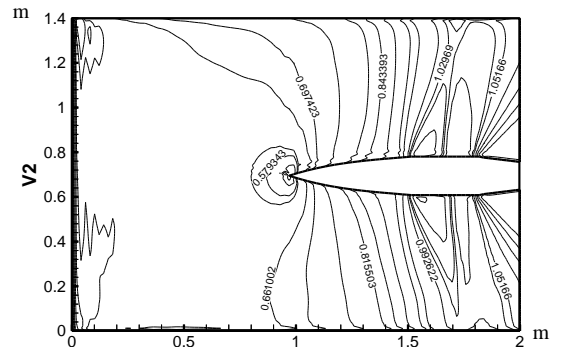


Fig. 5. Machconture, SOCBT, M=0. 94

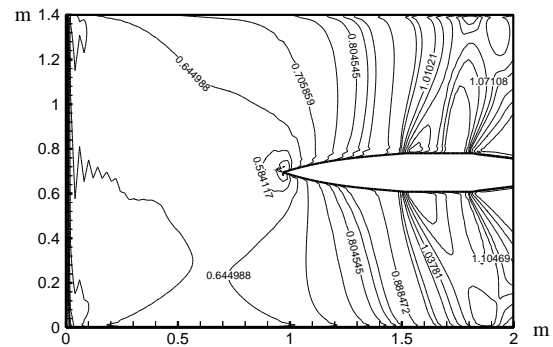


Fig.6. Machconture, SOCBT, M=0.96.

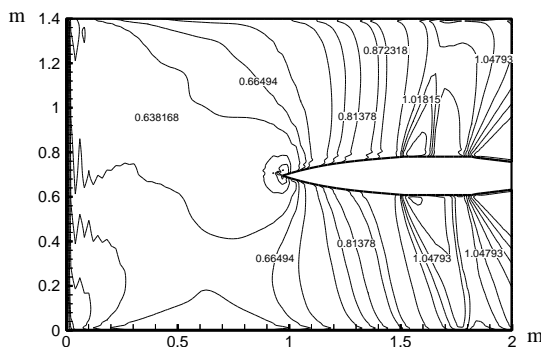


Fig.3. Machconture, SOCBT, M=0.9.

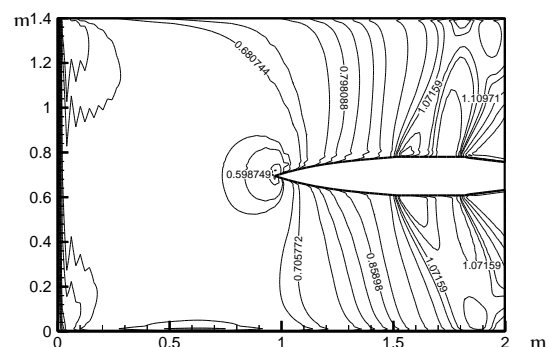
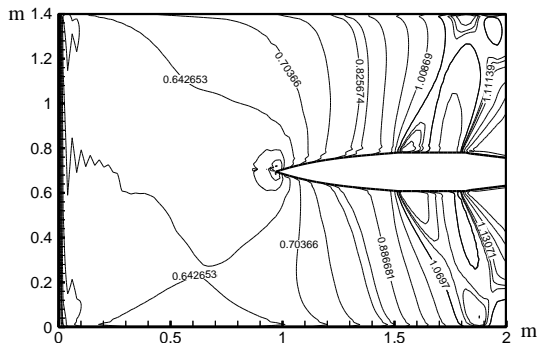


Fig.7. Machconture, SOCBT, M=0.98.



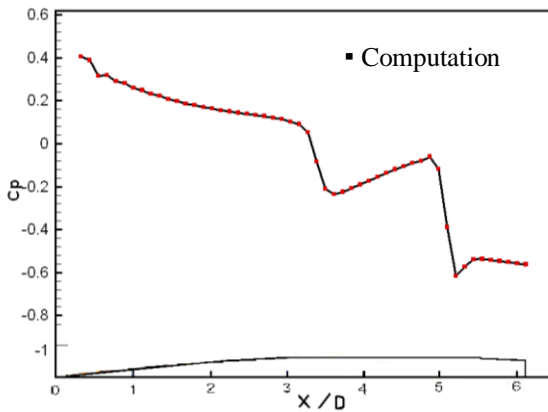


Fig.12a. Longitudinal Surface Pressure Distribution, OSCBT, Projectile, $M_\infty=0.96$, $\alpha=4$ deg, Lee Side.

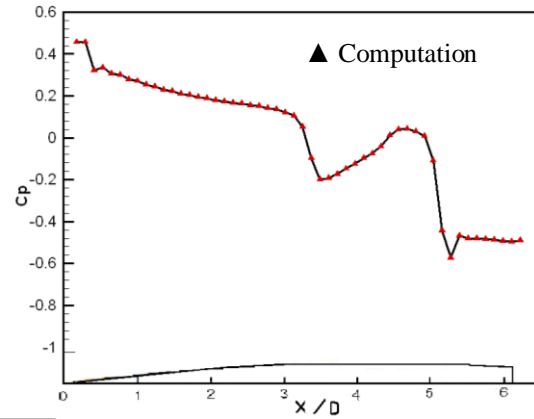


Fig.12b. Longitudinal Surface Pressure Distribution, OSCBT, Projectile, $M_\infty=0.96$, $\alpha=4$ deg, Wind Side.

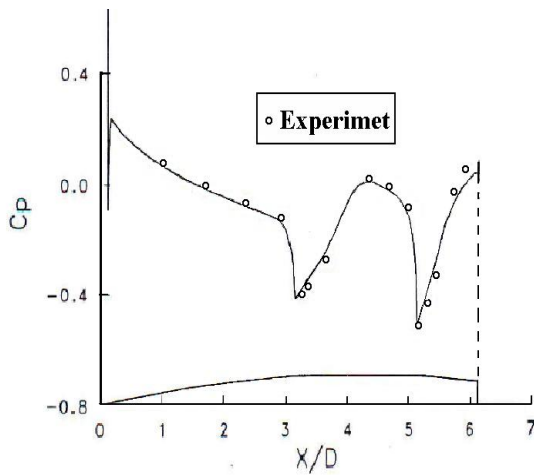


Fig.13a. Longitudinal Surface Pressure Distribution, OSCBT Projectile, $M_\infty=0.96$, $\alpha=4$ deg, Lee Side.

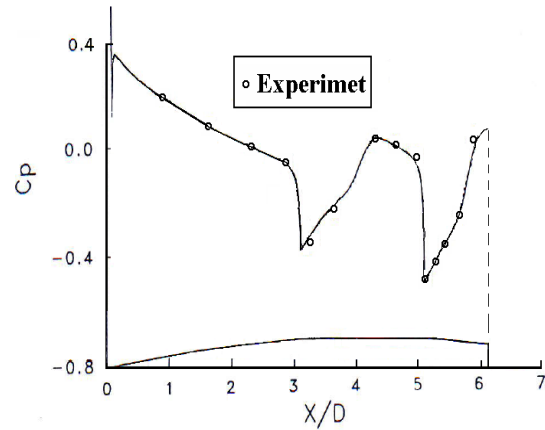


Fig.13b. Longitudinal Surface Pressure Distribution, OSCBT Projectile, $M_\infty=0.96$, $\alpha=4$ deg, Wind Side.

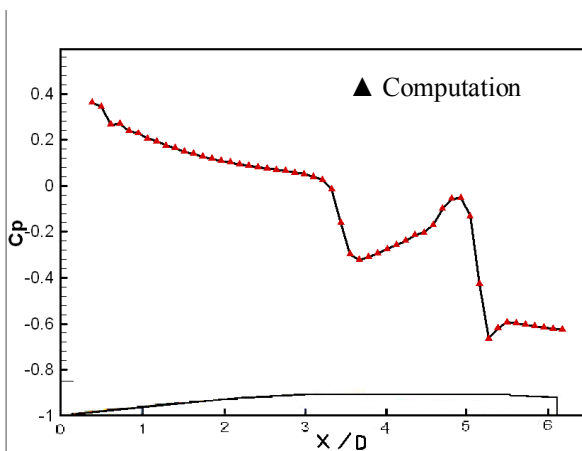


Fig.14a Longitudinal Surface Pressure Distribution, OSCBT, Projectile, $M_\infty=0.90$, $\alpha=4$ deg, Lee Side.

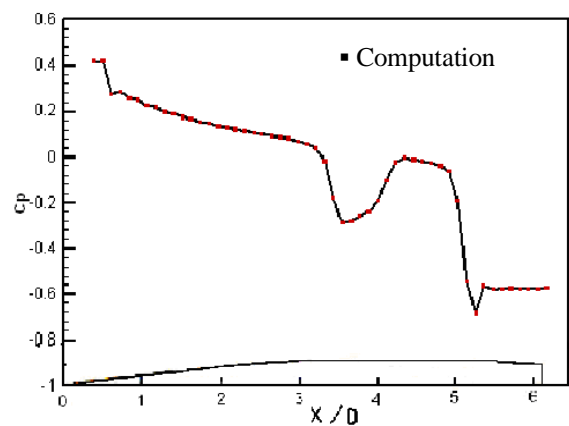


Fig.14b Longitudinal Surface Pressure Distribution, OSCBT, Projectile, $M_\infty=0.90$, $\alpha=4$ deg, Wind Side.

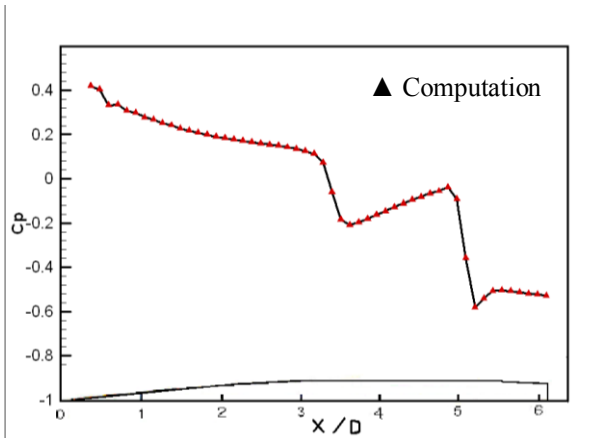


Fig.15a Longitudinal Surface Pressure Distribution, OSCBT Projectile, $M_\infty=0.98$, $\alpha=4$ deg, Lee Side.

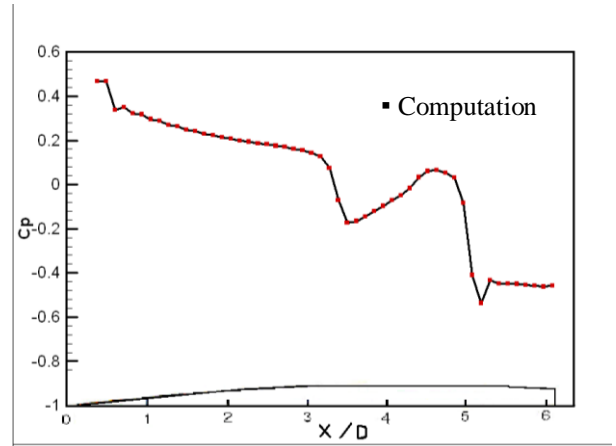


Fig.15b Longitudinal Surface Pressure Distribution, OSCBT, Projectile, $M_\infty=0.98$, $\alpha=4$ deg, Wind Side.

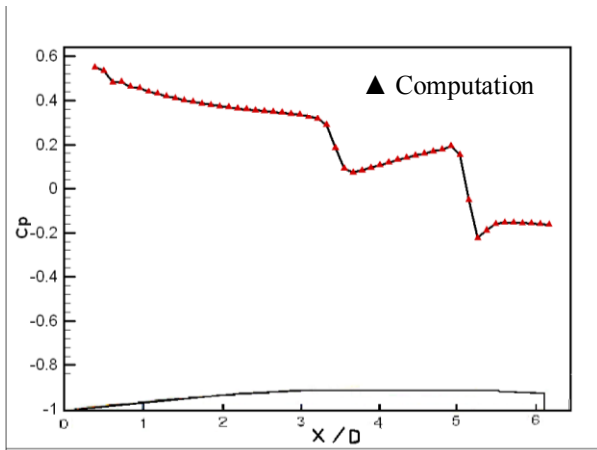


Fig.16a Longitudinal Surface Pressure Distribution, OSCBT, Projectile, $M_\infty=1.20$, $\alpha=4$ deg, Lee Side.

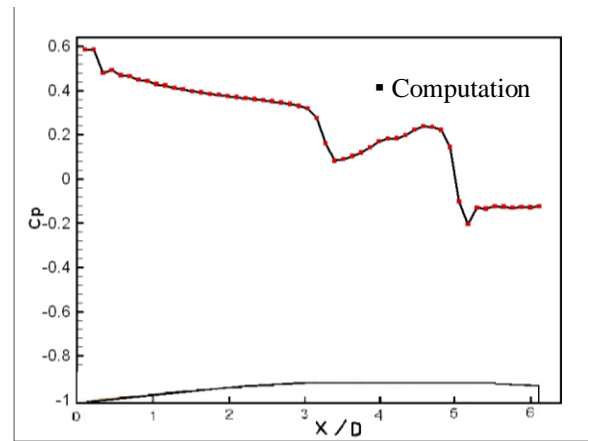


Fig.16b Longitudinal Surface Pressure Distribution, OSCBT, Projectile, $M_\infty=1.20$, $\alpha=4$ deg, Wind Side.

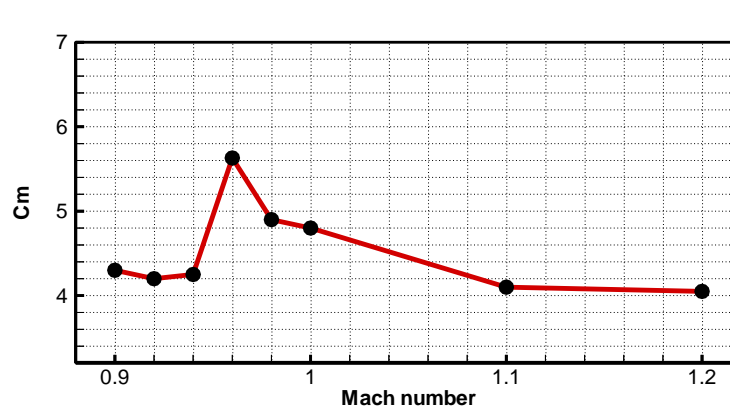


Fig.17. Slope of Pitching Moment Coefficient, c_m & Mach Number, SOCBT Projectile.

4. Conclusions

1. The implementation of MacCormack's scheme succeeded in predicting the mixed subsonic-supersonic flow domain, which is important in the study of numerical computations of transonic critical aerodynamic behavior.
2. The conservation form of partial differential equations has succeeded in predicting the location, strength of the shock wave (capturing the shock wave), and the properties at the flow field upstream and downstream of the normal shock.
3. The value of 0.8 for Courant-Fredrichs-Lewy (CFL) factor is used successfully for solving explicit Euler equations.
4. Body fitted coordinates have succeeded in the prediction of flow characteristic through the complex boundary.
5. The base region of a projectile should be included in the numerical computational analyses to find the optimum projectile account.

Notation

a	Speed of sound
CFL	Courant Friedrichs Lewy number of Stability
e	Specific internal energy
e_t	Total specific energy
E, F, U	Column vector in Cartesian coordinate
$\overline{E, F, U}$	Column vector in body filled coordinate
J	Jacobian of coordinate transformation
P	Static pressure
t	Time
u	Velocity component in x Coordinate direction
\overline{U}	Conservation velocity component in η coordinate direction
\overline{V}	Conservation velocity component in ξ coordinate direction
v	Velocity component in y coordinate direction
x	Cartesian coordinate

y Cartesian coordinate

Greek letters

Δt	Time step
ρ	Density
$\Delta x, \Delta y$	Spatial steps in physical domain
$\Delta \xi, \Delta \eta$	Spatial steps in computational domain
ξ, η	Computational coordinates

Subscript

x , y	Spatial derivative
ξ, η	Computational derivative

Superscript

t	Time level
t+ Δt	Next time level

5. References

- [1] Deiwert, G. S., "Numerical Simulation of Three Dimensional Boattail Afterbody Flow Field," *AIAA Journal*, Vol. 19, May 1981, pp.582-588.
- [2] Nietubicz, C. J., Sturek, W. B., and Heavey, K. R., "Computations of Projectiles Magnus Effect at Transonic Velocities, A *IAA Journal*, Vol. 23, No. 7, July 1985 pp. 998-1004.
- [3] Nietubicz, C. J., Sahu, J., and Lafarge, R., "Aerodynamic Coefficient Predictions for a Projectile Configuration at Transonic Speeds, "U.S. Army Ballistic Research Laboratory, Aberdeen Proving Ground, MD, BRL-MR-3639' Dec. 1987.
- [4] Sahu, J., Nietubicz C. J., and Steger, J.L., " Computations of Projectile Base Flow With and Without Base Injection, "U.S. Army Ballistic Research Laboratory, Aberdeen Proving Ground, MD, ARBRL-TR-02532N, Nov. 1983. (ADA135738) also *AIAA Journal*, Vol. 23, No.9, Sept. 1985, pp. 1348-1355.
- [5] Sahu, J., "Three Dimensional Base Flow Calculation for a Projectile at Transonic Velocity, "A *IAA Paper* 86-1051, May 1986.

- [6] Benek, J. A., Steger, J. L., Dougherty, F. C., and Buning, P. G., "A Three-Dimensional Chimera Grid Embedding Technique," *AIAA Paper* 85-1523, July 1985.
- [7] Belk, D. M., and Whitfield. D. L., "Three-Dimensional Euler Solutions on Blocked Grids Using an Implicit Two-Pass Algorithm," *AIAA Paper* 87-0450, Jan. 1987.
- [8] Raymer, D.P. "Aircraft Design: A conceptual Approach", 2nd Edition *AIAA Education Series*, Washington 1992.
- [9] JOHN. D. ANDERSON, TR., "Computational Fluid Dynamics", Department of Aerospace Engineering University of Maryland, McGraw-Hill, New York, International Editions 1995.
- [10] KLAUS A. HOFFMANN, "Computational Fluid Dynamics for Engineers". The University of Texas at Austin, A Publication of Engineering Education System™, Austin, Texas 78713, USA.
- [11] Nietubicz, C. J., Sturek, W. B., and Heavey, K. R., "Computations of Projectiles Magnus Effect at Transonic Velocities," *AIAA Journal*, Vol. 23, No. 7, July 1985p, p. 998-1004.
- [12] Kayser, L. D., and Whiton, F., "Surface Pressure Measurements on a Boattailed Projectile Shape at Transonic Speeds," U.S. Army Ballistic Research Laboratory, Aberdeen Proving Ground, MD, ARBRL-MR-03161, March 1982 (AD A113520).
- [13] Bangent, L.H., Santman, D.M., and Miller, L.D., "Some Effects of cruise speed and Engine Matching on Supersonic Inlet Design", *Aircraft Journal*, Vol.19, No.1, Jan. 1982.
- [14] Moretti, and Gino, "Efficient Euler Solver With Many applications" *AIAA Journal*, Vol. 26, No.6, p.p. 755-757, June 1988.
- [15] Dimitri P., Diffuser Performance of Two-Stream Supersonic Wind Tunnels", *AIAA Journal* Vol.27, No.8, Aug. 1989.
- [16] Sigh Th. R., Chandran B.S.S., Belou V., and Sundaraagan, T., "Numerical Simulation of Supersonic Mixed Compression Axisymmetric Air Intakes", NCABE, Dec.2000.
- [17] الأستاذ الدكتور منذر اسماعيل الدروبي "مبادئ ديناميكا الغازات" الأستاذ في جامعة بغداد قسم الهندسة الميكانيكية (الطبعة المنقحة) 1987.
- [18] Jubaraj Sahu U.S. "Numerical Computations of Projectiles and Experimental work " Army Ballistic Research laboratory, Aberdeen Proving Ground, Maryland 21005-5066 *AIAA Journal*, Vol. 28, No. 5, May 1990, pp. 807-816.

الحسابات العددية في المنطقة الصوتية الحرجة لعوامل ديناميك الهواء لمقذوفه سلاح المدفعية

أحمد فؤاد مهدي كريدي

قسم هندسة عمليات التصنيع/ كية هندسة الخوارزمي/ جامعة بغداد

الخلاصة

أن تحديد عوامل ديناميك الهواء من قبل مصممين الشكل الخارجي للمقذوفات هي خطوة حاسمة في تطوير أي نوع من المقذوفات إن من أهم الأمور هي تحديد عوامل ديناميك الهواء للسرعات القريبة من سرعة الصوت حيث أن سلوك ديناميك الهواء الحرج يظهر في نظام السرعة القريبة من سرعة الصوت ويتم مراقبة التغير السريع في عوامل ديناميك الهواء . وقد تم إجراء حساب مجال جريان ذات البعدين في المنطقة الانتقالية (القريبة من سرعة الصوت) باستخدام الحل الجبري اللوغارتمي استنادا إلى طريقة الاختلاف المحدد بأسلوب تقنية ماكورماك لحل معادلة أويلر لدراسة مشكلة تدفق الهواء في المنطقة المختلطة فوق الصوتية ودون الصوتية وقد تم تحديد تفاصيل وقيم الموجات الصدمية الغير متناظرة وقد تم مقارنة الضغوط المحسوبة على السطح مع البيانات التجريبية العملية و كانت متقاربة بشكل جيد. وتم حساب تأثير معامل عزم الانقلاب على الطيران الحر للمقذوف للمناطق الحرجة الصوتية وتأثيرها على طيران المقذوف.